SCIENCE CHINA
Technological Sciences

Special Topic: High Entropy Alloys
• Review •

February 2018 Vol.61 No.2: 168–178
https://doi.org/10.1007/s11431-017-9137-4

Fatigue behavior of high-entropy alloys: A review

CHEN PeiYong[1], LEE Chanho[1], WANG Shao-Yu[1], SEIFI Mohsen[2], LEWANDOWSKI John J[2], DAHMEN Karin A[3], JIA HaoLing[1], XIE Xie[1], CHEN BiLin[1], YEH Jien-Wei[4], TSAI Che-Wei[4], YUAN Tao[5] & LIAW Peter K[1*]

[1] *Department of Materials Science and Engineering, The University of Tennessee, Knoxville 37996, USA;*
[2] *Department of Materials Science and Engineering, Case Western University, Cleveland 44106, USA;*
[3] *Department of Physics, University of Illinois, Urbana 61801, USA;*
[4] *Department of Materials Science and Engineering, 'National' Tsing Hua University, Hsinchu 30013, Taiwan, China;*
[5] *Department of Industry and System Engineering, Ohio University, Athens 45701, USA*

Received April 1, 2017; accepted August 28, 2017; published online November 15, 2017

Fatigue failures cost approximately 4% of the United States' gross domestic product (GDP). The design of highly fatigue-resistant materials is always in demand. Different from conventional strategies of alloy design, high-entropy alloys (HEAs) are defined as materials with five or more principal elements, which could be solid solutions. This locally-disordered structure is expected to lead to unique fatigue-resistant properties. In this review, the studies of the fatigue behavior of HEAs during the last five years are summarized. The four-point-bending high-cycle fatigue coupled with statistical modelling, and the fatigue-crack-growth behavior of HEAs, are reviewed. The effects of sample defects and nanotwins-deformation mechanisms on four-point-bending high-cycle fatigue of HEAs are discussed in detail. The influence of stress ratio and temperature on fatigue-crack-growth characteristics of HEAs is also discussed. HEAs could exhibit comparable or greater fatigue properties, relative to conventional materials. Finally, the possible future work regarding the fatigue behavior of HEAs is suggested.

high-entropy alloys, fatigue behaviour, statistical modelling, fatigue crack growth

Citation: Chen P Y, Lee C, Wang S Y, et al. Fatigue behavior of high-entropy alloys: A review. Sci China Tech Sci, 2018, 61: 168–178, https://doi.org/10.1007/s11431-017-9137-4

1 Introduction

Fatigue—a phenomenon that happens when materials are subjected to cyclic loading, which accumulates damage during their service and causes failure. The total cost of fatigue to the economy of the United States was $ 119 billion in 1982, nearly 4% of the GDP in that year [1]. Even nowadays, the failure caused by fatigue still bring enormous loss to the society. Therefore, it is greatly economically beneficial to design excellent fatigue-resistant structural materials and study their fatigue behaviors. The past research, which is related to the development of fatigue-resistant materials, mainly focuses on the conventional structural alloys, such as aluminum alloys, steels, titanium-based alloys, nickel-based alloys, and so on. The above alloys are designed, following the rules: with higher strength, more ductility, and less manufacture defects, fatigue properties will be enhanced. Along with the traditional alloys-design strategies, the presence of second phases and precipitates may greatly affect the fatigue behavior [2–5].

Challenging the traditional alloy-design strategy, a new alloy field, high-entropy alloys (HEAs), has merged in recent years. HEAs defined as materials that have at least five principal elements with the concentration of each element rang-

*Corresponding author (email: pkliaw@utk.edu)

ing from 5 at. % (atomic percent) to 35 at. % in the aspect of compositions [6–13]. Another definition, which is in the concept of entropy, is that HEAs are alloys which have configurational entropy greater than 1.5*R* (*R* (gas constant)=8.314 J/K mol) [14–16]. The high-entropy effect resulted from complex compositions could simplify alloy structures and form solid solutions, including face-centered cubic (FCC) [8,12,17–19], body-centered cubic (BCC) [8,12,20], or hexagonal closed-pack (HCP) [8,12,21–24] structures. HEAs can be single phase or multi-phase materials [6,8,20]. The previous studies during the last decades have shown that HEAs have promising properties, such as high strength and hardness, superior resistance to wear, corrosion, oxidation, etc. [8,12,25–29]. Moreover, as more HEAs systems are designed and investigated, exceptional properties are characterized, such as high fracture toughness, fatigue resistance, and thermal stability [5,7,8,18,30–32]. The above advantages make HEAs attractive in industrial fields.

Based on the recent studies on fatigue behavior of HEAs, this article reviewed the high-cycle fatigue behavior and fatigue-crack-growth characteristics of HEAs, coupled with various statistical analysis methods. The effects of defects and nanotwins during deformation on fatigue behavior are discussed in detail. The influence of stress ratio (defined later) and temperature on the fatigue-crack-growth characteristics is also discussed. Furthermore, suggested future work is proposed, to obtain the fundamental understanding of the fatigue behavior of HEAs.

2 Review

2.1 Four-point-bending high-cycle fatigue

2.1.1 Effect of defects on fatigue behavior

It is well known that mechanical processing, i.e., cold rolling, could greatly improve the strength of materials. However, during mechanical processing, more defects are induced into the materials and, thus, crack initiation is easily to be formed. In fact, in the studies of fatigue behavior of structural materials, the defects induced during manufacturing or processing are always the critical issues.

Hemhill et al. [5] firstly investigated the effect of defects on the high-cycle fatigue behavior of the $Al_{0.5}CoCrCuFeNi$ HEAs by four-point-bending high-cycle fatigue experiments with a stress ratio 0.1. The concept of stress ratio is defined as

$$R = \frac{\sigma_{\min}}{\sigma_{\max}}, \quad (1)$$

where $\sigma_{\min}$ is the minimum loading, and $\sigma_{\max}$ is the maximum loading. The $Al_{0.5}CoCrCuFeNi$ HEAs were prepared by arc melting, then annealed at 1000 °C for 6 h, water quenched, and cold rolled. The phenomenon of scattering of some fatigue data was also observed. A possible cause for the scattering data may be the defect variations in different samples, which were introduced during the casting or cold-rolling process. Figure 1 shows the scanning-electron-microscopy (SEM) results coupled with the energy-dispersive X-ray spectroscopy (EDS) analysis on the $Al_{0.5}CoCrCuFeNi$ fatigue sample. Aluminum-oxide particles were found in the samples. These particles were believed to cause stress concentration and provide nucleation sites for crack initiation. Thus, the fatigue resistance was decreased. The authors also found that the scattering data could be divided into two groups that one of which was a strong group with better fatigue endurance, while the other was a weak group with worse fatigue performance. More detailed statistical analysis regarding these two groups will be discussed in sect. 2.1.3 [5].

The surface condition of the fatigue samples could greatly affect the fatigue behavior of the materials [5]. Cracks are usually initiated at the defects that exist on the surface of the sample, or at the corners of the samples where stress concentration leads to crack initiation. In the study of Hemphill et al. [5], the fracture surface was examined, as shown in Figure 2(a). Typical characteristics of fatigue-fracture surfaces, such as crack-initiation sites, crack propagation, and final fracture, are demonstrated. Figure 2(b) presents that microcracks, which formed from the surface of the samples, were observed, leading to crack-initiation behavior.

2.1.2 Effects of nanotwins on fatigue behavior

Based on the previous work by Hemphill et al. [5], Tang et al. [32] further investigated the deformation mechanism of the as-rolled $Al_{0.5}CoCrCuFeNi$ HEAs during four-point-bending-fatigue experiments by the focus-ion-beam (FIB) and transmission-electron microscopy (TEM). As reported in the study, three different locations from the samples, including the crack-initiation site, an adjacent region to the crack-initiation site, and a region away from the crack-initiation site, were examined. Low-density nanotwins have already existed in the samples before the fatigue tests, which were believed to be introduced due to the cold-rolled process. However,

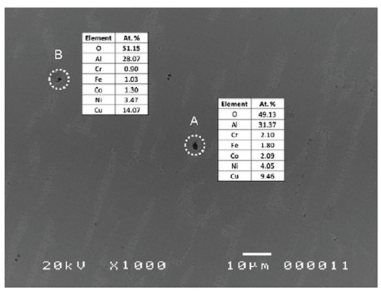

Figure 1 SEM image coupled with the EDS analysis. The labeled A and B indicated the presence of aluminum-oxides particles [5].

more nanotwins were observed at the crack-initiation site, compared with the other two sites. Figure 3 illustrates the investigation on the FIB sample at the crack-initiation site. Two different-orientation sets of dense nanotwins coupled with a large amount of tangled dislocations were observed, as presented in Figure 3(a). Orientations of the two-set nanotwins, which were identified as $[2\bar{1}1]$ and $[21\bar{1}]$ directions, were illustrated in Figure 3(b) and (c). The first set of the nanotwins are shown in Figure 3(d) and (e) with the direction of $[2\bar{1}1]$, while Figure 3(f) shows the other set with the direction of $[21\bar{1}]$ [32].

2.1.3 *Predictive models for fatigue life*

The relationship between the fatigue life of materials and applied stress is an important factor to consider in the design-for-reliability process [33]. Fatigue data are often illustrated in the form of a *S*-*N* curve where the applied stress range or stress amplitude, *S*, is plotted versus fatigue life, *N*, which is expressed in cycles to failure. In the *S*-*N* curve, the term, "fatigue-endurance limit", is commonly defined to be the stress level below which the failure of the samples will not occur before large number of cycles (e.g., 10^7 or 10^8 cycles). In the fatigue study, data-analysis methods are very necessary to study the fatigue behavior. The current predictive models that are applied on the fatigue behavior will be introduced below [5,32].

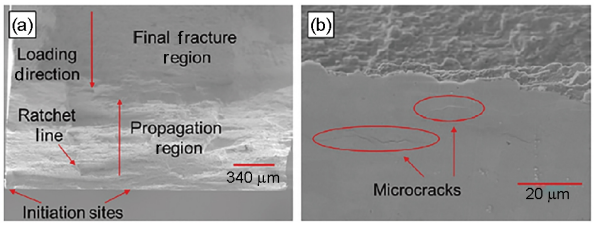

Figure 2 (a) SEM examination of the fracture surface of a failed sample; (b) crack initiation found on the sample surface and below the fatigue-fracture plane [5].

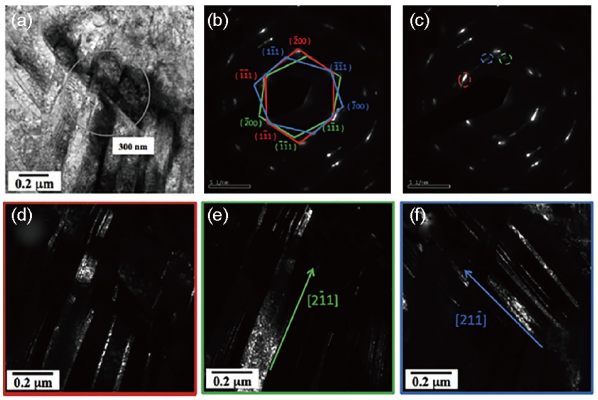

Figure 3 (a) Two sets of nanotwins with a high density of tangled dislocations; (b) three sets of diffraction patterns with a zone axis of [011]; (c) two orientations of nanotwins and the matrix are indicated; (d) dark-field image of the first set of nanotwins; (e) the first set of nanotwins (arrow); and (f) the second set of nanotwins (arrow) [32].

(1) Weibull predictive model.

Hemphill et al. [5] firstly used the Weibull predictive model to quantify the fatigue behavior of the HEA $Al_{0.5}CoCrCuFeNi$. In this model, the Weibull distribution is assumed in each fixed stress range to describe the fatigue-life distribution, based on a commonly-used eq. (2)

$$N(S) = cS^{(-d)}, \tag{2}$$

where S is the applied stress range, $N(S)$ denotes the expected number of fatigue-life cycles at S, c and d are positive materials parameters. Taken the natural logarithm, eq. (2) becomes

$$\log(N(S)) = \gamma_0 + \gamma_1 \log(S), \tag{3}$$

where $\gamma_0 = \log(c)$ and $\gamma_1 = -d$. Eqs. (2) and (2) provide a simple way to describe the *S*-*N* relation. However, they ignore the data scattering in the *S*-*N* curve as observed. An error term, ε, is introduced into eq. (3) to describe the variability of the fatigue data

$$\log(N(S)) = \gamma_0 + \gamma_1 \log(S) + \varepsilon, \tag{4}$$

the error term, ε, is assumed to follow the standardized smallest extreme-value distribution. Using eq. (4), the original fatigue-life model becomes a Weibull regression model [5,34]. Eq. (4) can be equivalently written as a Weibull-accelerated life testing model that is widely used in the reliability analysis of engineering [5,34–36]. Following the Weibull distribution, the probability density function (PDF) and the cumulative distribution function (CDF) are, respectively, described by eqs. (5) and (6)

$$f(N(S) \mid \alpha(S), \beta) = \frac{\beta}{\alpha(S)} \left(\frac{N(S)}{\alpha(S)} \right)^{\beta - 1} \exp\left[-\left(\frac{N(S)}{\alpha(S)} \right)^{\beta} \right], \tag{5}$$

$$F(N(S) \mid \alpha(S), \beta) = 1 - \exp\left[-\left(\frac{N(S)}{\alpha(S)} \right)^{\beta} \right], \tag{6}$$

where $\alpha(S)$ is the Weibull-scale parameter that follows $\log(\alpha(S)) = \gamma_0 + \gamma_1 \log(S)$, and β denotes the Weibull-shape parameter.

If the fatigue samples had not failed when the four-point-bending-fatigue tests were terminated at 10^7 cycles, they are termed censored observations in this model [22]. The probability to obtain a censored observation at a stress range S is

$$P(N(S) \geq N_c) = 1 - F(N(S) \mid \alpha(S), \beta) = \exp\left[-\left(\frac{N(S)}{\alpha(S)} \right)^{\beta} \right], \tag{7}$$

where N_c denotes the censor time of the experiment. Here N_c equals 10^7. There are three unknown parameters, γ_0, γ_1, and

β, in the Weibull-predictive model, which can be estimated by the maximum likelihood estimation model [5,34]. The fatigue-experimental data can be denoted by i=1, 2, …, m [5]. Then, the maximum likelihood estimation method estimates the three parameters by maximizing the likelihood function,

$$L(\gamma_0,\gamma_1,\beta)=\prod_{i=1}^{m}\left[\frac{\beta}{e^{\gamma_0+\gamma_1\log(S_i)}}\left(\frac{N_i}{e^{\gamma_0+\gamma_1\log(S_i)}}\right)^{\beta-1}\right]^{\delta_i}\times\exp\left[-\left(\frac{N_i}{e^{\gamma_0+\gamma_1\log(S_i)}}\right)^{\beta}\right], \tag{8}$$

where m is the total number of tested samples, N_i and S_i are fatigue-life cycles and the applied stress range to the ith sample. If the sample is regarded as a censored observation, δ_i=0, and otherwise, δ_i=1.

In this model, the quantile life is used to describe the relation between the fatigue life and the applied stress range, which is given by

$$N_p(S)=\exp[\gamma_0+\gamma_1\log(S)][-\log(1-p)]^{1/\beta}. \tag{9}$$

The median fatigue life is adopted to describe the relationship between the average fatigue life and applied stress [5,36]. A 95%-predictive interval for fatigue life is constructed by the 0.025 and 0.975 quantiles to illustrate the variety of the *S*-*N* curve. Figure 4 shows the predicted median fatigue life, which is between 0.025 and 0.975 quantiles [5]. All the failure observations are captured by the 95%-predictive interval in this model.

(2) Weibull-mixture model.

To better analyze the excessive data variability, Hemphill et al. [5] used the Weibull-mixture predictive model, which is a combination of two Weibull predictive models. In this integrated model, the fatigue data are divided into two groups, a strong group and a weak group. The authors assumed that the data variability is related to the defect density in the HEA-fatigue samples. A mixture of two Weibull distributions is applied to different groups in this model at each stress range. The PDF and CDF of the Weibull mixture model are given, respectively, in eqs. (10) and (11)

$$f\left(N(S)\mid p,\alpha_w(S),\beta_w,\alpha_s(S),\beta_s\right)=p\frac{\beta_w}{\alpha_w(S)}\left[\frac{N(S)}{\alpha_w(S)}\right]^{\beta_w-1}\exp\left(-\left[\frac{N(S)}{\alpha_w(S)}\right]^{\beta_w}\right)+(1-p)\frac{\beta_s}{\alpha_s(S)}\left[\frac{N(S)}{\alpha_s(S)}\right]^{\beta_s-1}\exp\left(-\left[\frac{N(S)}{\alpha_s(S)}\right]^{\beta_s}\right), \tag{10}$$

$$F\left(N(S)\mid p,\alpha_w(S),\beta_w,\alpha_s(S),\beta_s\right)=p\left(1-\exp\left(-\left[\frac{N(S)}{\alpha_w(S)}\right]^{\beta_w}\right)\right)+(1-p)\exp\left(-\left[\frac{N(S)}{\alpha_s(S)}\right]^{\beta_s}\right), \tag{11}$$

where the subscripts, w and s, in the parameters denote the weak and strong groups, respectively, and p represents the fraction of the samples that belong to the weak group. By applying the maximum likelihood method, which is the same method as in the Weibull-predictive model, the p-quantile fatigue lives of the weak and strong groups are given by

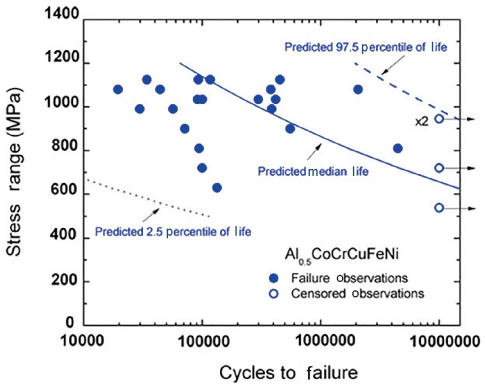

Figure 4 (Color online) Predicted quantile lives of the $Al_{0.5}CoCrCuFeNi$ HEA with the Weibull-predictive model [5].

$$N_{p,w}(S)=\exp[\gamma_{w,0}+\gamma_{w,1}\log(S)][-\log(1-p)]^{1/\beta_w}, \tag{12}$$

$$N_{p,s}(S)=\exp[\gamma_{s,0}+\gamma_{s,1}\log(S)][-\log(1-p)]^{1/\beta_s}. \tag{13}$$

Figure 5 illustrates the predicted quantile lives by the Weibull-mixture predictive models. The data points are divided into two groups where the circle dots group (weak) and the squars group (strong) are described by eqs. (12) and (13), respectively.

Figure 6 presents that on average the strong group tends to have less defects, compared with the weak group, which is corresponding to the calculation results by the Weibull-mixture model [22]. With fewer defects, the HEA samples tend to have longer fatigue lives under cyclic loading.

(3) Random endurance-limit fatigue-life model.

Tang et al. [32] adopted the random endurance-limit fatigue-life model to study the *S*-*N* curve of the $Al_{0.5}CoCrCuFeNi$ HEA. Considering the fatigue-endurance limits, a commonly-used equation on the *S*-*N* curves is given by [32]

$$n=\begin{cases}c(s-\gamma)^{-d}, s>\gamma,\\ \infty, \quad s\le\gamma,\end{cases} \tag{14}$$

where γ denotes the fatigue-endurance limits, and, c and d are positive materials parameters. Taking the natural logarithm on eq. (14)

$$\log(n)=\begin{cases}\gamma_0+\gamma_1\log(s-\gamma), s>\gamma,\\ \infty, \quad s\le\gamma,\end{cases} \tag{15}$$

where $\gamma_0=\log(c)$ and $\gamma_1=-d$, which are similar to the Weibull predictive model above. A random error term, ε, is also introduced into eq. (15)

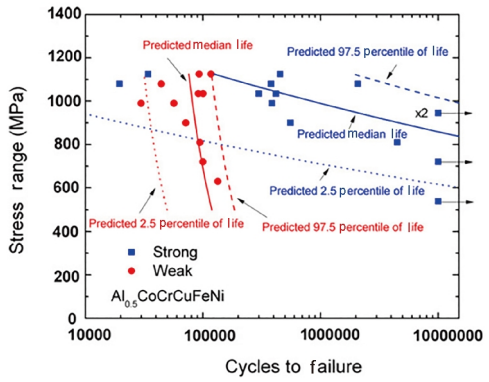

Figure 5 (Color online) Predicted quantile lives of the $Al_{0.5}CoCrCuFeNi$ HEA with the Weibull-mixture-predictive model [5].

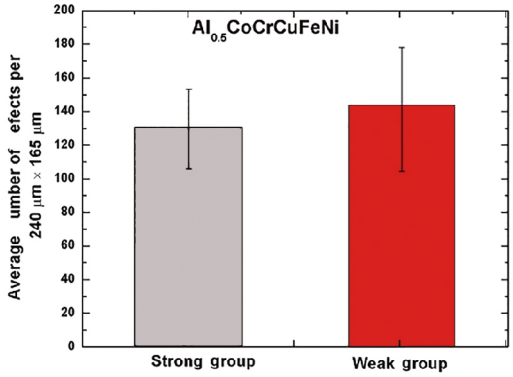

Figure 6 (Color online) Column figures of the average number of defects for the strong and weak groups [5].

$$\log(n) = \gamma_0 + \gamma_1 \log(s - \gamma) + \varepsilon, s > \gamma, \tag{16}$$

here the fatigue-endurance limit, γ, is assumed to follow a probability distribution, $V=\log(\gamma)$. Suppose that V follows a PDF, which is given by

$$f_v(v;\mu_\gamma;\sigma_\gamma) = \frac{1}{\sigma_\gamma}\varphi_V\left(\frac{v-\mu_\gamma}{\sigma_\gamma}\right), \tag{17}$$

where μ_γ denotes the location parameter, and σ_γ represents the scale parameter. Assume that $x=\log(S)$, and $W=\log(N(S))$. For a fixed value of $V<x$, the conditional PDF of W is given by

$$f_{W|V}(w;\gamma_0,\gamma_1,\sigma,x,v) = \frac{1}{\sigma}\varphi_{W|V}\left(-\frac{w-[\gamma_0+\gamma_1\log(\exp(x)-\exp(v))]}{\sigma}\right), \tag{18}$$

where $\gamma_0+\gamma_1\log(\exp(x)-\exp(v))$ is the location parameter, and σ is the scale parameter. Here $\varphi_{W|V}$ is assumed to be the standardized normal or smallest extreme value of PDF. The marginal PDF of W is given by

$$f_W(w;x,\theta) = \int_{-\infty}^{x}\frac{1}{\sigma\sigma_y}\varphi_{W|V}\left(\frac{w-[\gamma_0+\gamma_1\log(\exp(x)-\exp(v))]}{\sigma}\right) \times\varphi_V\left(\frac{v-\mu_\gamma}{\sigma_y}\right)\mathrm{d}v, \tag{19}$$

where $\theta=(\gamma_0, \gamma_1, \sigma, \mu_\gamma, \sigma_\gamma)$. The marginal CDF of W is given by

$$F_W(w;x,\theta) = \int_{-\infty}^{x}\frac{1}{\sigma_y}\phi_{W|V}\left(\frac{w-[\gamma_0+\gamma_1\log(\exp(x)-\exp(v))]}{\sigma}\right) \times\varphi_V\left(\frac{v-\mu_\gamma}{\sigma_y}\right)\mathrm{d}v, \tag{20}$$

where $\phi_{W|V}(\cdot)$ is the conditional CDF of W. The maximum likelihood method is also applied to estimate the unknown parameters.

Tang et al. [32] then used this model to analyze three conditions of the $Al_{0.5}CoCrCuFeNi$ HEA samples, to see how the purity of the HEA elements and defects of the samples affect the scatter of the fatigue data. The HEAs in all three conditions are homogenized at 1000°C for 6 h, water quenched, and then cold rolled [32]. The detailed information of the three conditions, including materials purity and machining, is listed in Table 1 [32]. Figure 7 shows the $f(\gamma; \mu_\gamma, \sigma_\gamma)$ functions for the three conditions of the $Al_{0.5}CoCrCuFeNi$ HEA samples. The curve of Condition 3 is the most narrow, which suggests that the samples fabricated with higher purity and less macro defects before cold rolling tend to have much less data scatter [32].

2.2 Fatigue-crack-growth behavior

The propagation of a crack takes up most of the fatigue life of materials. To study the fatigue behavior of materials, the fatigue-crack-growth-rate test is commonly used. The obtained parameters during the test include the crack length (a), the number of cycles (N), the range of cyclic stress ($\Delta\sigma$), and the stress-intensity-factor range (ΔK). For the specimen with a specific size, the stress-intensity-factor range, ΔK, is given by

Table 1 Detailed information of the three conditions of the $Al_{0.5}CoCrCuFeNi$ HEA [32]

Condition	Materials purity (in wt.%)	Machining
Condition 1	>99%	Shrinkage pores and macrosegregation could be found in some portion of the samples
Condition 2	>99%	Shrinkage pores and macrosegregation were removed before cold rolling
Condition 3	High purity: >99.9%	Shrinkage pores and macrosegregation were removed before cold rolling

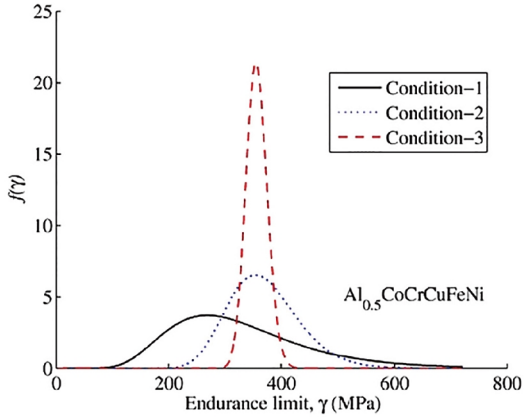

Figure 7 (Color online) Probability distributions of the endurance limits for the three conditions of $Al_{0.5}CoCrCuFeNi$ HEAs as reported [32].

$$\Delta K = b\Delta\sigma(\pi a)^{1/2}, \tag{21}$$

where b is a dimensionless parameter that depends on the geometry and a is the crack length. ΔK can also be given by the difference between the maximum stress-intensity factor, K_{max}, and the minimum stress-intensity factor, K_{min}. The fatigue-crack growth can usually be divided into three stages: near threshold, steady stage, and fast fracture. In Stage I, with low ΔK values, the fatigue-crack propagation is very slow. For example, the near-threshold crack-propagation rate da/dN ranges from 10^{-10}–10^{-8} m/cycle. A parameter, ΔK_{th}, is defined as the stress-intensity-factor range below which the fatigue crack would not grow or propagate at an extremely slow rate. The fatigue-threshold stress-intensity-factor range, ΔK_{th}, depends on the stress ratio. In the condition of a same maximum loading, as the stress ratio increases, the fatigue threshold decreases because of the higher mean stress at greater R values, which results in less crack closure and larger effective stress-intensity-factor range, ΔK_{eff} [37–39]. The definition of ΔK_{eff} is given by

$$\Delta K_{eff} = K_{max} - K_{cl}, \tag{22}$$

where K_{cl} is the crack-closure stress-intensity factor. In Stage II, as the stress-intensity-factor range increases to a mid-region, the $\log(da/dN)$ versus $\log\Delta K$ is approximately linear. Stage II is usually the largest region of the fatigue-crack-growth curve. The Paris-Erdogan law is commonly used to describe this stage, which is given by

$$\frac{da}{dN} = C(\Delta K)^n, \tag{23}$$

where N is the number of load cycles, C and n are material constants. At high stress intensities, which refer to Stage III, the crack grows rapidly to the final failure of the materials.

2.2.1 *Multi-phase HEAs*

Seifi et al. [31] investigated the fatigue-crack-growth behavior of the as-cast HEAs, $Al_{0.2}CrFeNiTi_{0.2}$ and $AlCrFeNi_2Cu$. The two compositions are characterized as the BCC+FCC phases by X-ray diffraction (XRD). The fatigue-crack-growth tests were conducted with conditions that are in the room-temperature air with the relative humidity of 40% at a cyclic frequency of 20 Hz, in accordance with the American Society for Testing and Materials International (ASTM) E647 [40]. As reported, the ΔK_{th} of $Al_{0.2}CrFeNiTi_{0.2}$ is 16 MPa $\sqrt{m}$ (R=0.1), while the ΔK_{th} of $AlCrFeNi_2Cu$ reaches 17 MPa $\sqrt{m}$ (R=0.1). Both $Al_{0.2}CrFeNiTi_{0.2}$ and $AlCrFeNi_2Cu$ showed a stress-ratio effect on ΔK_{th}, where the increase in R produced a great reduction in ΔK_{th} and an increase in the Paris' law slope. This fatigue-crack-propagation characteristics of the as-cast $Al_{0.2}CrFeNiTi_{0.2}$ and $AlCrFeNi_2Cu$ are similar to the metallic alloys, such as γ-TiAl alloys, and metal-matrix-composite systems, such as Al-Zu-Mg-Cu with SiC particles, where the Paris slopes at low R values greatly increase with increasing R [31,41–44]. The $Al_{0.2}CrFeNiTi_{0.2}$ and $AlCrFeNi_2Cu$ HEAs showed much higher fatigue-threshold values of 16 and 17 MPa $\sqrt{m}$, respectively, at a low R of 0.1, relative to metallic alloys, such as Ti-6Al-4V, and bulk metallic glass (BMG), such as $Zr_{41.2}Ti_{13.8}Cu_{12.5}Ni_{10}Be_{22.5}$, as shown in Table 2 [31,45–49]. The stress-ratio effect that the fatigue threshold decreases as stress ratio increases is also observed. This trend is likely due to the fatigue-crack closure produced by the large fracture-surface roughness at a low value of R, which increases the crack-closure level and decreases the ΔK_{eff} and results in a larger ΔK_{th} at the low R [37–39,50]. A summary of the fatigue-crack-growth threshold results of the HEAs under different stress ratios is demonstrated in Table 2 [31].

The SEM characterization on the fracture surface of $AlCrFeNi_2Cu$ is shown in Figure 8, while the $Al_{0.2}CrFeNiTi_{0.2}$ exhibits similar properties. Fatigue striations appear in the Paris-law regime (Stage II), as shown in Figure 8(a). Dimple-like ductile features are presented in the overload region, as exhibited in Figure 8(b). Figure 8(c) and (d) illustrates the combination of brittle and dimple-like ductile features. For the multiphase HEAs systems, the combination of brittle and dimple-like ductile features of the two HEAs compositions correspond to the sizes and volume fractions of BCC and FCC phases, respectively [31].

2.2.2 *Single-phase HEA*

Temperature effects on the fatigue-crack-growth behavior of a single-phase HEA, CrMnFeCoNi, were studied by Thurston et al. [45]. The CrMnFeCoNi samples are heat treated at 1473 K for 48 h after induction melting, then rotary swaged at room temperature and recrystallized at 1073 K for 1 h [45]. The fatigue-crack-growth experiments of the CrMnFeCoNi HEA show a fatigue threshold ΔK_{th}, of ~4.8 MPa $\sqrt{m}$ at 293 K, while the ΔK_{th} increases to ~6.3 MPa $\sqrt{m}$ at a lower temperature of 198 K. The threshold values of the CrMnFeCoNi at both 293 and 198 K are comparable with some other conventional alloys, such as Ti-6Al-4V and some low alloy

Table 2 Summary of the fatigue-crack-growth testing parameters and threshold results of HEAs and conventional materials

Composition	Temperature	Stress ratio	Frequency (Hz)	ΔK_{th} (MPa $\sqrt{m}$)
HEA-AlCrFeNi$_2$Cu [31]	RT	0.1	20	17
HEA-AlCrFeNi$_2$Cu [31]	RT	0.3	20	5
HEA-AlCrFeNi$_2$Cu [31]	RT	0.7	20	7
HEA-Al$_{0.2}$CrFeNiCu$_{0.2}$ [31]	RT	0.1	20	16
HEA-Al$_{0.2}$CrFeNiCu$_{0.2}$ [31]	RT	0.3	20	7
HEA-Al$_{0.2}$CrFeNiCu$_{0.2}$ [31]	RT	0.7	20	5
HEA-CrMnFeCoNi [45]	293 K	0.1	25	~4.8
HEA-CrMnFeCoNi [45]	198 K	0.1	25	~6.3
$Zr_{41.2}Ti_{13.8}Cu_{12.5}Ni_{10}Be_{22.5}$ [46]	295 K	0.1	25	~3
Ferritic steel [47]	RT	0.1	20	~9
2NiCrMoV [48]	296 K	0.1	90	8.9
3.5NiCrMoV [48]	296 K	0.1	90	7.8
Ti-6Al-4V [49]	298 K	0.1	50	~4.7

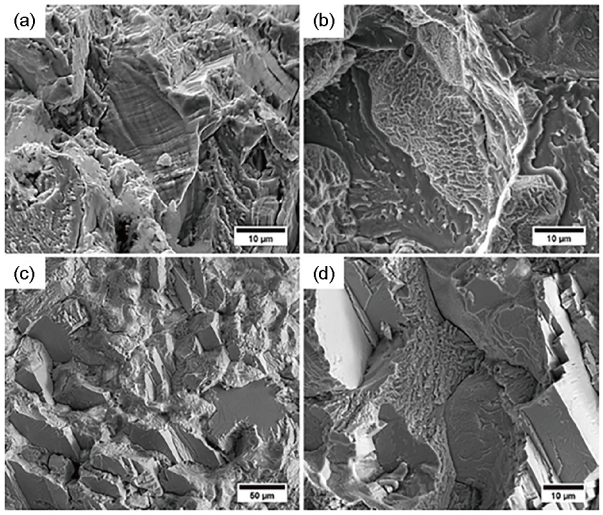

Figure 8 SEM images of the fracture surfaces of the AlCrFeNi$_2$Cu HEA. (a) Fatigue-striation- features in the ΔK regime (10 ~ 15 MPa $\sqrt{m}$); (b) dimple-like ductile features in the ΔK regime (10–15 MPa $\sqrt{m}$); (c) and (d) combined with brittle and dimple-like ductile features in the ΔK regime (beyond 20 MPa $\sqrt{m}$) [31].

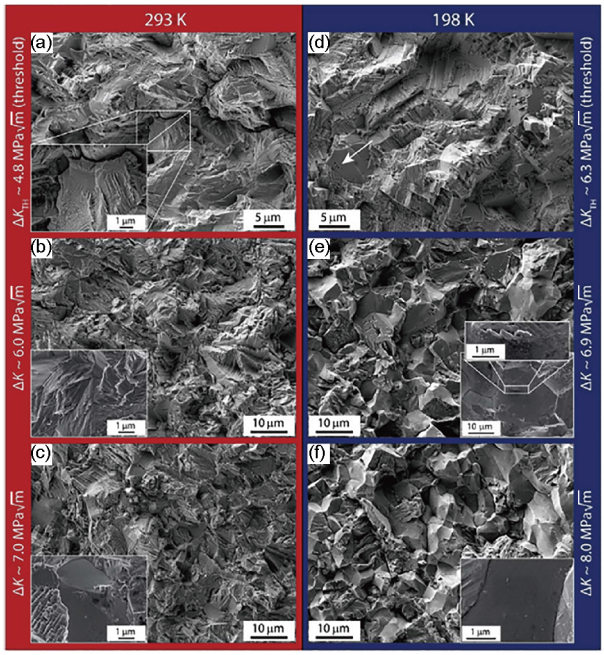

Figure 9 (Color online) Fracture morphology of CrMnFeCoNi at 293 and 198 K. (a)–(c) Fracture surfaces of samples tested at 293 K exhibit transgranular crack propagation with minor intergranular crack propagation; (d) serrated surfaces with sharp edges are observed and indicate a planar-slip deformation mechanism; (e), (f) fracture surfaces of samples tested at 198 K mainly exhibit intergranular crack propagation [45].

steels, as shown in Table 2. Further microstructural characterization reveals that the transgranular fracture is the dominating crack-propagation mode at room temperature, while the fatigue-crack growth is predominated by the intergranular fracture at cryogenic temperature. Figure 9 shows the fracture surface examination of CrMnFeCoNi tested at 293 and 198 K [50]. The transgranular crack propagation coupled with minor intergranular crack propagation is observed in Figure 9(a)–(c), with the samples tested at 293 K. Figure 9(d) shows the fracture morphology at 198 K, where the serrated fracture with sharp edges is observed, indicating that planar slip is regarded as another deformation mechanism during fatigue-crack propagation. Figure 9(e) and (f) illustrates that the intergranular fracture mainly occurred at 198 K. The authors believe that the intergranular fracture leads to the neighboring crack flanks to have more physical contact, which results in enhancing the roughness-induced fatigue crack-closure effect and giving a higher ΔK_{th} at a lower temperature, as mentioned in previous studies [37,51]. Thus, the fatigue threshold is increased at the cryogenic temperature, compared to that at room temperature. The fatigue-crack-growth rates of the single-phase CrMnFeCoNi are similar to those of the twinning-induced-plasticity

(TWIP) steels, for the reasons that the CrMnFeCoNi and TWIP steels all exhibited a lack of twining in fatigue experiments at room temperature [45]. Also, they have comparable fatigue threshold and Paris slopes [45].

3 Discussion

3.1 Relationship between defects and life cycles

The effect of defects on fatigue behavior of HEAs was studied by the experimental and computational results [5,32]. Fewer defects (gas pores, inclusions, precracks, etc.) tend to lead to a stronger fatigue resistance. Therefore, it is of great importance to control defects during the fabrication and mechanical processing for future developments and applications. The HEA study of Hemphill et al. [5] also suggests that a reduction in defects could lead to a more favorable fatigue resistance, compared with that of conventional structural materials.

3.2 Deformation mechanisms during four-point-bending fatigue

Nanotwins coupled with tangled dislocations, which are introduced due to the cold-rolling process, exist prior to fatigue-crack initiation of the FCC-matrix $Al_{0.5}CoCrCuFeNi$ HEA samples and have been observed by previous studies [32,52]. In the comparison of the three different locations (the crack-initiation site, adjacent to the crack-initiation site, and away from the crack-initiation site) of the four-point-bending-fatigue HEA samples, more nanotwins were found in the crack-initiation site where severe deformation took place. Nanotwinning is believed to be the main plastic-deformation mechanism of the $Al_{0.5}CoCrCuFeNi$ HEAs before fatigue-crack initiation and during crack propagation. The nanotwin-deformation mechanism under an applied stress or after rolling is also observed in other FCC or FCC-matrix HEAs, such as the CrMnFeCoNi, AlCoCuFeNi, FeNiCoCrMn, etc. [53–56].

Moreover, these nanotwins strengthened the HEAs and gave high fatigue limits [32]. Twin boundaries were formed due to the formation of the nanotwins, which increased the interfaces and thus reduced the dislocation mean-free path, resulting in greater strength at larger fatigue limits [32]. This twinning-induced strengthening also occurs in the case of the austenitic stainless-steel thin film [57]. The formation of nanotwins is believed to be mainly due to the high matrix strength and low stacking fault energy (SFE) for the present $Al_{0.5}CoCrCuFeNi$ HEAs [32,52]. The former is related to solution strengthening and Widmanstatten precipitates strengthening [52]. The latter is attributed to that the SFE declines with increasing the concentration of solutes for the reason of Suzuki interaction [52]. The $Al_{0.5}CoCrCuFeNi$ HEAs with the FCC matrix contain a large number of solutes, which may tend to have even lower SFE and thus, promote the formation of nanotwins.

3.3 Comparison of the HEA fatigue performance with other alloys

The HEAs show great fatigue resistance, compared with other conventional alloys. Figure 10(a) of the fatigue-endurance limit versus ultimate tensile strength (UTS) indicates that HEAs have relative high-endurance limits, compared with conventional structural alloys, as reported by Tang et al. [32]. Note that for structural materials, as the UTS increases, the fatigue-endurance limits (EL) tend to increase [5,32]. Most of the alloys in Figure 10(a) follow the rule that the EL approximately equals 0.24UTS [5,32]. However, HEAs could reach the upper bound of EL with 0.35UTS [5,32]. Tang et al. [32] use another term, fatigue ratio, which is defined as the ratio of the fatigue-endurance limit to the UTS, to further compare the fatigue properties between HEAs and other alloys. As shown in Figure 10(b), the lower points of the fatigue ratios of the HEAs are at the same level, compared with those of Ti alloys, steels, Ni alloys, and Mg-alloys. However, the upper bound is greatly higher than other alloys in the figure. Overall, both Figure 10(a) and (b) suggests that HEAs can have great fatigue strengths for structural applications [32].

3.4 Comparison of HEA fatigue-crack-growth behavior of other alloys

Compared with some of other conventional alloys, the HEAs are comparable or even better in the aspects of fatigue-crack-growth properties [31,45]. Figure 11 of the fatigue-crack growth, da/dN, versus stress intensity range, ΔK, presents the single-phase CrMnFeCoNi HEAs and the two Al-containing multi-phase HEAs, compared with the low-alloy rotor steels of 2NiCrMoV and 3.5NiCrMoV, ferritic steel of Fe-0.07C-0.08Si-0.46Mn-0.02P-0.039S (in wt. %), Ti-6Al-4V, and bulk metallic glass (BMG) of $Zr_{41.2}Ti_{13.8}Cu_{12.5}Ni_{10}Be_{22.5}$ (in at. %) [46–49]. The conditions of all the data in Figure 11 are listed in Table 2. The CrMnFeCoNi HEAs are comparable with other conventional alloys under room temperature and even cryogenic temperature, in terms of the fatigue threshold and crack-growth rate in the Paris regime. Compared to several conventional alloys, the whole crack-growth-rate curves of Al-containing HEAs locate on the right-hand side of the da/dN versus ΔK plot, relative to other materials in the figure. The values of ΔK_{th} of Al-containing HEAs are much greater than those of other alloys in the Figure 11 and Table 2.

Notice that as pointed out by Thurston et al. [45], the difference of ΔK_{th} between the CrMnFeCoNi HEAs and the Al-containing HEA may be caused by the variation of the as-cast structure and the annealing structure, due to the increase of the fracture-surface roughness with the as-cast

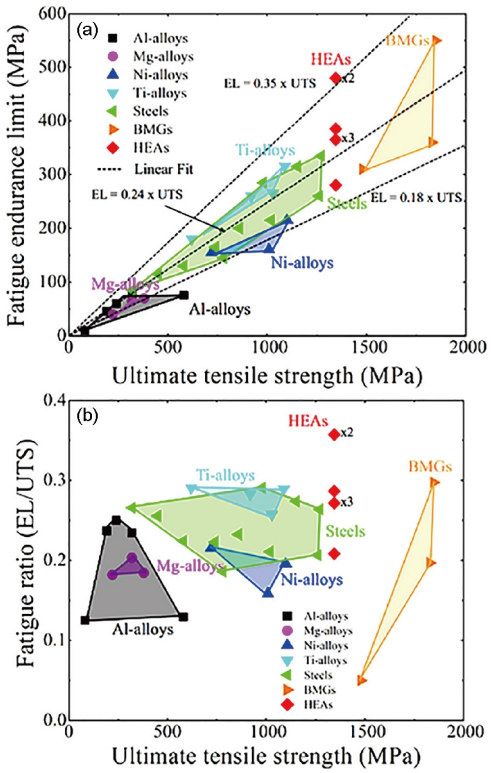

Figure 10 (Color online) Fatigue-performance comparison of $Al_{0.5}CoCrCuFeNi$ HEAs and other conventional alloys. (a) Stress amplitude of fatigue-endurance limit versus UTS; (b) fatigue ratio versus UTS [5,32].

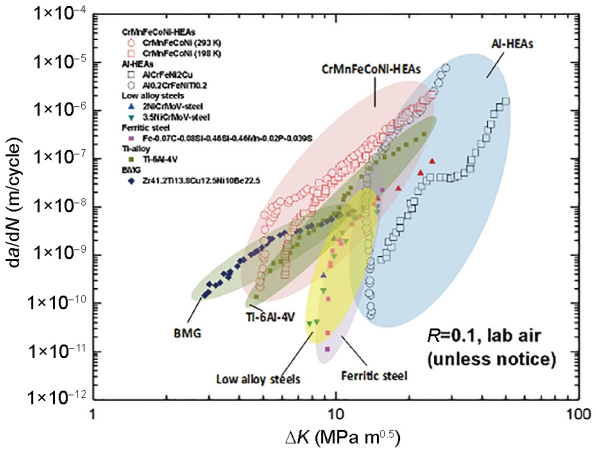

Figure 11 (Color online) da/dN-ΔK curves comparing the CrMnFeCoNi HEA and the Al-containing HEAs ($AlCrFeNi_2Cu$ and $Al_{0.2}CrFeNiTi_{0.2}$) with other conventional alloys and bulk metallic glass of $Zr_{41.2}Ti_{13.8}Cu_{12.5}Ni_{10}Be_{22.5}$ [31,45,46–49].

structure and the sample size used for testing on the Al-containing HEAs. The surface roughness could induce the crack closure and results in a higher ΔK_{th} value [50,58–60]. The as-cast Al-containing HEAs show a higher microhardness of even 510 HV, compare to ~375 HV of the CrMnFeCoNi (the same condition as the samples used in fatigue-crack-growth tests) [31,61,62]. The difference of the microstructure and mechanical behavior of the CrMnFeCoNi and the Al-containing HEAs could cause the varied fatigue-crack-growth behavior, which still need further studies.

4 Suggested future work

Up to the present time, the investigation on the fatigue behavior of HEAs is limited. Based on the previous work discussed above, a fundamental, in-depth understanding of the fatigue behavior of HEAs is in great demand for potential applications of HEAs. The following future investigations are suggested.

(1) So far, only four-point-bending high-cycle fatigue tests and fatigue-crack-growth experiments are conducted on HEAs concerning fatigue-behavior investigation. Despite the convenience of four-point-bending high-cycle fatigue, the detailed fatigue-fracture mechanisms of four-point-bending fatigue need to be further studied. It is essential to have the in-depth fracture-mechanism knowledge. Thus, the fundamental understanding on the fatigue-deformation mechanism and life prediction could be provided for structural applications. Moreover, tensile-fatigue-behavior studies are suggested to obtain more comprehensive investigations.

(2) Due to the great phase stability and high strength at elevated temperatures, coupled with great corrosion resistance [26,28,63], HEAs have promising future applications in some extreme environments. The fatigue behavior at elevated temperatures and in corrosion environments should be investigated systematically for the future development of HEAs.

(3) Most of the above fatigue studies are on multiphase HEAs. So far, the fundamental understanding on the fatigue-deformation mechanism of single-phase HEAs is still lacking. Thus, more fatigue investigations on single-phase HEAs with excellent mechanical properties are suggested.

(4) Recent studies show that refractory HEAs (r-HEAs) have exhibited superior properties, such as ultra-high strength, great ductility, single phase, etc. The r-HEAs present huge potential for future applications in industries. Yet no related fatigue studies have been published. Therefore, the fatigue-behavior investigations on r-HEAs are suggested to obtain the in-depth understanding of fatigue performance.

(5) It is very interesting to see that the as-cast Al-containing HEAs ($Al_{0.2}CrFeNiTi_{0.2}$ and $AlCrFeNi_2Cu$) have superior near-threshold fatigue-crack-growth behavior and ΔK_{th}, relative to conventional alloys. However, the rates of near-threshold fatigue-crack-growth and ΔK_{th} of the CrMnFeCoNi are comparable to conventional materials. Thus, it is very important to further study the difference between the as-cast Al-containing HEAs and the CrMnFeCoNi HEA.

5 Conclusions

This article reviews the investigation during the last five years on the fatigue behavior of HEAs. The effects of defects and nanotwins on four-point-bending high-cycle fatigue behavior of HEAs, and, the fatigue-crack-growth characterizations of HEAs, have been reviewed and discussed. The pertinent conclusions are summarized below.

(1) The defects of the HEA-fatigue samples, which are introduced during manufacturing and processing, could greatly influence the fatigue resistance of HEAs. Statistical analysis reveals that fatigue samples with less defects tend to have stronger fatigue resistance.

(2) Nanotwinning is the main plastic-deformation mechanism for the $Al_{0.5}CoCrCuFeNi$ HEAs before crack initiation and propagation, which strengthens the fatigue resistance of the HEAs with greater fatigue-endurance limits, and fatigue ratios.

(3) The fatigue-crack-growth behavior of the two as-cast HEAs, $Al_{0.2}CrFeNiTi_{0.2}$ and $AlCrFeNi_2Cu$, exhibited the stress-ratio effect. As the stress ratio, R, increases, the threshold values greatly decrease. The fractography shows that brittle and dimple-like ductile features correspond to the multiphase structures. The single-phase HEA CrMnFeCoNi displays temperature effects on the fatigue-crack-growth behavior, with fatigue threshold increased at a lower temperature. The temperature effect is attributed to the change of the crack-propagation mechanism from the transgranular to intergranular fracture mode, which results in enhancing the roughness-induced crack closure and giving a higher ΔK_{th} at a lower temperature.

(4) Compared to conventional alloys, HEAs could show comparable or greater fatigue-endurance limits, fatigue ratio, and fatigue-crack-growth properties, which suggest promising future applications in industries. However, further research needs to be conducted to study fatigue performance of HEAs in depth.

This work was supported by the Department of Energy (DOE), Office of Fossil Energy, National Energy Technology Laboratory (Grant No. DE-FE-0024054, DE-FE-0011194), the U.S. Army Research Office Project (Grant No. W911NF-13-1-0438), the National Science Foundation (DMR-1611180), the QuesTek Innovation LLC (limited liability company), the Ministry of Science and Technology of Taiwan (Grant No. MOST 105-2221-E-007-017-MY3), the Department of Materials Science and Engineering at the National Tsing Hua University (Taiwan), the School of Materials Science and Engineering of the Dalian University of Technology, China.

1 Reed R P. The Economic Effects of Fracture in the United States. US Department of Commerce, National Bureau of Standards,1983
2 Nahm H, Moteff J. Second phase formation and its influence on the fatigue properties of incoloy 800 at elevated temperatures. Metallur Trans A, 1976, 7: 1473–1477
3 Vardiman R G, Kant R A. The improvement of fatigue life in Ti-6Al-4V by ion implantation. J Appl Phys, 1982, 53: 690–694
4 Lockyer S A, Noble F W. Fatigue of precipitate strengthened Cu-Ni-Si alloy. Mater Sci Tech, 1999, 15: 1147–1153
5 Hemphill M A, Yuan T, Wang G Y, et al. Fatigue behavior of $Al_{0.5}CoCrCuFeNi$ high entropy alloys. Acta Mater, 2012, 60: 5723–5734
6 Yeh J W, Chen S K, Lin S J, et al. Nanostructured high-entropy alloys with multiple principal elements: Novel alloy design concepts and outcomes. Adv Eng Mater, 2004, 6: 299–303
7 Santodonato L J, Zhang Y, Feygenson M, et al. Deviation from high-entropy configurations in the atomic distributions of a multi-principal-element alloy. Nat Commun, 2015, 6: 5964
8 Zhang Y, Zuo T T, Tang Z, et al. Microstructures and properties of high-entropy alloys. Prog Mater Sci, 2014, 61: 1–93
9 Cantor B, Chang I T H, Knight P, et al. Microstructural development in equiatomic multicomponent alloys. Mater Sci Eng-A, 2004, 375-377: 213–218
10 Guo S, Liu C T. Phase stability in high entropy alloys: Formation of solid-solution phase or amorphous phase. Prog Nat Sci-Mater Int, 2011, 21: 433–446
11 Ng C, Guo S, Luan J, et al. Entropy-driven phase stability and slow diffusion kinetics in an $Al_{0.5}CoCrCuFeNi$ high entropy alloy. Intermetallics, 2012, 31: 165–172
12 Gao M C, Yeh J W, Liaw P K, et al. High-Entropy Alloys: Fundamentals and Applications. Cham: Springer International Publishing, 2016
13 Zhang Y, Zhou Y J, Lin J P, et al. Solid-solution phase formation rules for multi-component alloys. Adv Eng Mater, 2008, 10: 534–538
14 Lu Z P, Wang H, Chen M W, et al. An assessment on the future development of high-entropy alloys: Summary from a recent workshop. Intermetallics, 2015, 66: 67–76
15 Carroll R, Lee C, Tsai C W, et al. Experiments and model for serration statistics in low-entropy, medium-entropy, and high-entropy alloys. Sci Rep, 2015, 5: 16997
16 Poletti M G, Branz S, Fiore G, et al. Equilibrium high entropy phases in X-NbTaTiZr (X=Al, V, Cr and Sn) multiprincipal component alloys. J Alloys Compd, 2016, 655: 138–146
17 Shun T T, Du Y C. Microstructure and tensile behaviors of FCC $Al_{0.3}CoCrFeNi$ high entropy alloy. J Alloys Compd, 2009, 479: 157–160
18 Gludovatz B, Hohenwarter A, Catoor D, et al. A fracture-resistant high-entropy alloy for cryogenic applications. Science, 2014, 345: 1153–1158
19 Li D, Li C, Feng T, et al. High-entropy $Al_{0.3}CoCrFeNi$ alloy fibers with high tensile strength and ductility at ambient and cryogenic temperatures. Acta Mater, 2017, 123: 285–294
20 Senkov O N, Wilks G B, Miracle D B, et al. Refractory high-entropy alloys. Intermetallics, 2010, 18: 1758–1765
21 Gao M C, Zhang B, Guo S M, et al. High-entropy alloys in hexagonal close-packed structure. Metall Mat Trans A, 2016, 47: 3322–3332
22 Feuerbacher M, Heidelmann M, Thomas C. Hexagonal high-entropy alloys. Mater Res Lett, 2015, 3: 1–6
23 Takeuchi A, Amiya K, Wada T, et al. High-entropy alloys with a hexagonal close-packed structure designed by equi-atomic alloy strategy and binary phase diagrams. JOM, 2014, 66: 1984–1992
24 Youssef K M, Zaddach A J, Niu C, et al. A novel low-density, high-hardness, high-entropy alloy with close-packed single-phase nanocrystalline structures. Mater Res Lett, 2015, 3: 95–99
25 Wu J M, Lin S J, Yeh J W, et al. Adhesive wear behavior of $Al_xCoCrCuFeNi$ high-entropy alloys as a function of aluminum content. Wear, 2006, 261: 513–519
26 Shi Y, Yang B, Liaw P. Corrosion-resistant high-entropy alloys: A review. Metals, 2017, 7: 43
27 Rao Z, Wang X, Wang Q, et al. Microstructure, mechanical properties, and oxidation behavior of $Al_xCr_{0.4}CuFe_{0.4}$ MnNi high entropy alloys . Adv Eng Mater, 2017, 19: 1600726
28 Shi Y, Yang B, Xie X, et al. Corrosion of $Al_xCoCrFeNi$ high-entropy

alloys: Al-content and potential scan-rate dependent pitting behavior. Corrosion Sci, 2017, 119: 33–45
29 Zuo T, Gao M C, Ouyang L, et al. Tailoring magnetic behavior of CoFeMnNiX (X= Al, Cr, Ga, and Sn) high entropy alloys by metal doping. Acta Mater, 2017, 130: 10–18
30 Zhang Z J, Mao M M, Wang J, et al. Nanoscale origins of the damage tolerance of the high-entropy alloy CrMnFeCoNi. Nat Commun, 2015, 6: 10143
31 Seifi M, Li D, Yong Z, et al. Fracture toughness and fatigue crack growth behavior of as-cast high-entropy alloys. JOM, 2015, 67: 2288–2295
32 Tang Z, Yuan T, Tsai C W, et al. Fatigue behavior of a wrought $Al_{0.5}$CoCrCuFeNi two-phase high-entropy alloy. Acta Mater, 2015, 99: 247–258
33 Pascual F G, Meeker W Q. Estimating fatigue curves with the random fatigue-limit model. Technometrics, 1999, 41: 277–289
34 Escobar A, Meeker Q. Statistical Methods for Reliability Data. New York: John Wiley & Sons, 1998
35 Meeker W Q, LuValle M J. An accelerated life test model based on reliability kinetics. Technometrics, 1995, 37: 133–146
36 Glaser R E. Estimation for a weibull accelerated life testing model. Naval Res Logistics, 1984, 31: 559–570
37 Liaw P K, Hudak S J, Donald J K. Influence of gaseous environments on rates of near-threshold fatigue crack propagation in nicrmov steel. Metallur Trans A, 1982, 13: 1633–1645
38 Liaw P K, Leax T R, Swaminathan V P, et al. Influence of load ratio on near-threshold fatigue crack propagation behavior. Scripta Metall, 1982, 16: 871–876
39 Liaw P K, Leax T R, Williams R S, et al. Near-threshold fatigue crack growth behavior in copper. Metallur Trans A, 1982, 13: 1607–1618
40 Standard Test Method for Measurement of Fatigue Crack Growth Rates. ASTM International, West Conshohocken, 2015
41 Zinsser Jr W A, Lewandowski J J. Effects of R-ratio on the fatigue crack growth of Nb-Si(ss) and Nb-10Si *in situ* composites. Metall Mat Trans A, 1998, 29: 1749–1757
42 Shang J K, Yu W, Ritchie R O. Role of silicon carbide particles in fatigue crack growth in SiC-particulate-reinforced aluminum alloy composites. Mater Sci Eng-A, 1988, 102: 181–192
43 El-Shabasy A. Effects of load ratio, R, and test temperature on fatigue crack growth of fully pearlitic eutectoid steel (fatigue crack growth of pearlitic steel). Int J Fatigue, 2004, 26: 305–309
44 Dahar M S, Seifi S M, Bewlay B P, et al. Effects of test orientation on fracture and fatigue crack growth behavior of third generation as-cast Ti-48Al-2Nb-2Cr. Intermetallics, 2015, 57: 73–82
45 Thurston K V S, Gludovatz B, Hohenwarter A, et al. Effect of temperature on the fatigue-crack growth behavior of the high-entropy alloy CrMnFeCoNi. Intermetallics, 2017, 88: 65–72
46 Gilbert C J, Ritchie R O, Johnson W L. Fracture toughness and fatigue-crack propagation in a Zr-Ti-Ni-Cu-Be bulk metallic glass. Appl Phys Lett, 1997, 71: 476–478
47 Masounave J, Baflon J P. Effect of grain size on the threshold stress intensity factor in fatigue of a ferritic steel. Scripta Metall, 1976, 10: 165–170
48 Stewart A T. The influence of environment and stress ratio on fatigue crack growth at near threshold stress intensities in low-alloy steels. Eng Fract Mech, 1980, 13: 463–478
49 Boyce B L, Ritchie R O. Effect of load ratio and maximum stress intensity on the fatigue threshold in Ti-6Al-4V. Eng Fract Mech, 2001, 68: 129–147
50 Suresh S, Ritchie R O. A geometric model for fatigue crack closure induced by fracture surface roughness. Metallur Trans A, 1982, 13: 1627–1631
51 Liaw P K, Saxena A, Swaminathan V P, et al. Effects of load ratio and temperature on the near-threshold fatigue crack propagation behavior in a CrMoV steel. Metallur Trans A, 1983, 14: 1631–1640
52 Tsai C W, Chen Y L, Tsai M H, et al. Deformation and annealing behaviors of high-entropy alloy $Al_{0.5}$CoCrCuFeNi. J Alloys Compd, 2009, 486: 427–435
53 Laplanche G, Kostka A, Horst O M, et al. Microstructure evolution and critical stress for twinning in the CrMnFeCoNi high-entropy alloy. Acta Mater, 2016, 118: 152–163
54 Sathiaraj G D, Bhattacharjee P P, Tsai C W, et al. Effect of heavy cryo-rolling on the evolution of microstructure and texture during annealing of equiatomic CoCrFeMnNi high entropy alloy. Intermetallics, 2016, 69: 1–9
55 Yu P F, Cheng H, Zhang L J, et al. Nanotwin's formation and growth in an AlCoCuFeNi high-entropy alloy. Scripta Mater, 2016, 114: 31–34
56 Wang Z, Baker I. Interstitial strengthening of a f.c.c. FeNiMnAlCr high entropy alloy. Mater Lett, 2016, 180: 153–156
57 Zhang X, Misra A, Wang H, et al. Nanoscale-twinning-induced strengthening in austenitic stainless steel thin films. Appl Phys Lett, 2004, 84: 1096–1098
58 Gray G T, Williams J C, Thompson A W. Roughness-induced crack closure: An explanation for microstructurally sensitive fatigue crack growth. Metallur Trans A, 1983, 14: 421–433
59 Llorca J. Roughness-induced fatigue crack closure: A numerical study. Fatigue Fracture Eng Mater Struct, 1992, 15: 655–669
60 Morris W L, James M R, Buck O. A simple model of stress intensity range threshold and crack closure stress. Eng Fract Mech, 1983, 18: 871–877
61 Gludovatz B, George E P, Ritchie R O. Processing, microstructure and mechanical properties of the CrMnFeCoNi high-entropy alloy. JOM, 2015, 67: 2262–2270
62 Yang J, Putatunda S K. Near threshold fatigue crack growth behavior of austempered ductile cast iron (ADI) processed by a novel two-step austempering process. Mater Sci Eng-A, 2005, 393: 254–268
63 Tang Z, Huang L, He W, et al. Alloying and processing effects on the aqueous corrosion behavior of high-entropy alloys. Entropy, 2014, 16: 895–911